Liquid Crystals
Publication details, including instructions for authors and subscription information:
http://www.informaworld.com/smpp/title~content=t713926090

High speed parallel synthesis of banana-shaped molecules and phase transition behaviour of 4-bromo-substituted derivatives

Sungmin Kang[a]; Jirakorn Thisayukta[a]; Hideo Takezoe[a]; Junji Watanabe Corresponding author[a]; Kumiko Ogino[b]; Takayuki Doi[b]; Takashi Takahashi[b]
[a] Department of Organic and Polymeric Materials, Tokyo Institute of Technology, Tokyo 152-8552, Japan [b] Department of Applied Chemistry, Tokyo Institute of Technology, Tokyo 152-8552, Japan

Online publication date: 19 May 2010

To cite this Article Kang, Sungmin , Thisayukta, Jirakorn , Takezoe, Hideo , Watanabe Corresponding author, Junji , Ogino, Kumiko , Doi, Takayuki and Takahashi, Takashi(2004) 'High speed parallel synthesis of banana-shaped molecules and phase transition behaviour of 4-bromo-substituted derivatives', Liquid Crystals, 31: 10, 1323 — 1336
To link to this Article: DOI: 10.1080/02678290412331298094
URL: http://dx.doi.org/10.1080/02678290412331298094

LIQUID CRYSTALS, VOL. 31, NO. 10, OCTOBER 2004, 1323–1336

High speed parallel synthesis of banana-shaped molecules and phase transition behaviour of 4-bromo-substituted derivatives

SUNGMIN KANG, JIRAKORN THISAYUKTA, HIDEO TAKEZOE, JUNJI WATANABE*

Department of Organic and Polymeric Materials, Tokyo Institute of Technology, Ookayama, Meguro-ku, Tokyo 152-8552, Japan

KUMIKO OGINO, TAKAYUKI DOI and TAKASHI TAKAHASHI

Department of Applied Chemistry, Tokyo Institute of Technology, Ookayama, Meguro-ku, Tokyo 152-8552, Japan

(*Received 16 January 2004; in final form 16 June 2004; accepted 23 June 2004*)

Novel derivative series of the well known bent-shaped P-*n*-O-PIMB liquid crystal mesogens, referred to as '4Br-P-*n*-O-PIMB', '4Cl-P-*n*-O-PIMB' and '5Cl-P-*n*-O-PIMB', having halogen atoms substituted on the phenyl ring in the central core, were synthesized by solution phase parallel synthesis based on a combinatorial approach. The mesomorphic behaviour and physical properties of all the new compounds were studied by means of optical microscopy, differential scanning calorimetry, X-ray and circular dichroism spectroscopy. We found interesting transitional behaviour for the 4Br-P-*n*-O-PIMB homologous series. The homologues with alkyl tails having carbon numbers of $n=3$–10, 12, 14 exhibit rather complicated mesomorphic behaviour, which is strongly sensitive to *n*. The chiral fluid smectic B2 phase with SmC_AP_A structure and unidentified smectic Bx phase were observed in the homologues with $n=9$, 10, 12, 14 and $n=3$–5, respectively. Interestingly, every member exhibits frustrated and/or helical ordered phases at low temperatures, designated as X1, X2, and X3 phases, which result from a spontaneous escape from a macroscopic polarization. The mesomorphic behaviour and mesophase structures differ remarkably from those of the parent P-*n*-O-PIMB homologues, suggesting that substitution of the halogen atoms at the central core essentially creates a particular interaction between molecules.

1. Introduction

Since the extraordinary properties such as ferroelectricity, chirality and frustration were observed in the smectic phases of achiral banana-shaped molecules P-*n*-O-PIMB **(1)** by Watanabe *et al.* [1–4], they have driven liquid crystal chemists and physicists into a new field of soft condensed matter. The nomenclature 'B phase' was established [5] to designate the mesophases formed by this type of molecule, and to date at least seven different kinds of B phases have been discovered. The first B phase discovered was the so-called B2 phase, which has been studied extensively. The layer structure of the B2 phase is characterized by the molecules stacking along the molecular tip with a tilt fashion in each layer, giving rise to a spontaneous polarization along the smectic strata. Initially, ferroelectric switching was reported for this phase by Watanabe *et al.* [1], but antiferroelectric switching behaviour was found to be a ground state structure of the B2 phase by Link *et al.* [6]. In the mean time, a large number of such materials have been synthesized, whose chemical structures are modified but based on P-*n*-O-PIMB homologues. Many approaches have involved the introduction of substituents into the central core of the molecules [7–17]. Apparently, the mesophase transition temperatures of these substituted P-*n*-O-PIMB derivatives are significantly decreased [8, 15]. Also, it is found that substitution strongly affects the mesophase behaviour [8, 16], which unusual shows polymorphism involving both of calamitic and banana phases simultaneously. The most common functional groups introduced into these P-*n*-O-PIMB-based mesogens are chloro, bromo and fluoro substituents; more recently, nitro, methoxy and methyl functional groups have also been used as substituents on the various positions of the phenyl central core. The results reveal many different kinds of mesomorphic behaviour varying from molecule to

*Author for correspondence:
e-mail: jwatanab@polymer.titech.ac.jp

Liquid Crystals ISSN 0267-8292 print/ISSN 1366-5855 online © 2004 Taylor & Francis Ltd
http://www.tandf.co.uk/journals
DOI: 10.1080/02678290412331298094

molecule, and the liquid crystalline properties are changed dramatically even though these substituents are introduced in the same position [8]. It is important that the substituents affect the bend angle of the central core, which is found to be a key factor in determining the mesomorphic behaviour of banana-shaped molecules [10].

In addition to the B2 phase, Thisayukta *et al*. have studied the alternative B phase, which is apparently a highly ordered smectic phase [7, 18]. The phase is called the B4 phase, which exhibits a texture reminiscent of chiral and/or helical structures. From X-ray and circular dichroic (CD) data, the structure of the B4 phase is proposed to be similar to that of the twisted grain boundary (TGB) phase. However, there is no clear evidence to support an unambiguous structural assignment of the B4 phase at present. Our interests focus on the origin of these chiral mesophases and of the fact that even though the classic bent-shaped P-*n*-O-PIMB molecules do not contain a chiral carbon, their mesophases are chiral. This has kept our focus on the origin of the chirality in such an achiral molecular system.

There are two arguments used to explain the origin of chirality in bent-shaped molecules: (1) a tilting of the bent-shaped molecules in the smectic strata, providing a macroscopic enantiomorphic structure [6, 19], and (2) a molecular twisted conformation adopted by the specific type of bent-shaped molecules. The latter is strongly supported by ^{13}C NMR [17, 20] and FTIR spectroscopies [21, 22], MO calculations [23] and our most recent work on a correlation of chirality between the B2 and B4 phases [24] for the P-*n*-O-PIMB homologous series. According to our investigation on the molecular conformation, it is clear that the central core of the molecule plays an important role on the mesomorphic behaviour in such a molecular system. Thus, we are interested in further modifying the central core to see how the substituents affect either the mesomorphic behaviour or mesophase structure.

In order to elucidate the effects of various substituents on a central core and for various lengths of alkyl tails, a high speed systematic synthesis of these derivatives is required. Combinatorial synthesis is currently one of the most interesting topics in, not only pharmaceutical development [25], but also in other fields of inorganic and organic chemistry [26], which provides a qualitative way to achieve this goal. Thus, it must be advantageous here to combine combinatorial chemistry and material science [27].

Thus we have undertaken the high speed parallel synthesis of a combinatorial library by the combination of central cores (resorcinol, 4-bromoresorcinol, 4-chlororesorcinol, and 5-chlororesorcinol) and terminal flexible chains with carbon numbers $n = 3$–10, 12, 14. In this paper, we report an efficient synthetic method for the substituted P-*n*-O-PIMB derivatives and the characterization of all the new compounds. Among these, we have found interesting transitional behaviour for the 4Br-P-*n*-O-PIMB homologues which differs greatly from that of the classic P-*n*-O-PIMB parent series. Specifically, we see the spontaneous formation of long range ordered phases in the low temperature region of these materials, the structures of which appear to be sensitive to the length of the terminal chains. The phase behaviour and mesophase structures of the 4Br-P-*n*-O-PIMB homologues will be discussed:

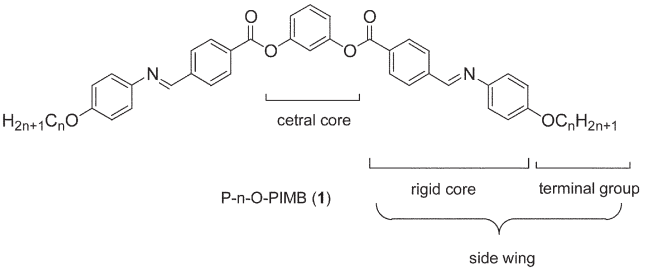

2. Experimental

2.1. *Characterization*

The optical microscopic textures of the materials were examined using an Olympus BX50 polarizing microscope equipped with a temperature-controlled Mettler Toledo FP82 hot stage. SAXS and WAXD measurements were performed using a Rigaku R-200 diffractometer with Cu Kα radiation. Transition temperatures of the whole series were measured using a Perkin-Elmer Pyris 1 differential scanning calorimeter (DSC).

2.2. *Synthesis*

2.2.1. *High speed parallel synthesis of a combinatorial library of banana molecules (**1**–**4**)*

The Shiff's base, imine moiety of P-*n*-O-PIMB derivatives is labile under acidic conditions while the phenol ester should be sensitive under nucleophilic conditions. Our plan of a high speed synthesis of P-*n*-O-PIMB derivatives **1** (X = H), **2** (X = 5-Cl), **3** (X = 4-Cl), **4** (X = 4-Br)) is illustrated in the scheme. Coupling of resorcinol derivatives **5A**–**5D**, 4-formylbenzoic acid (**6**), and 4-alkoxyanilines **8a**–**8j** provides a 40-member combinatorial library of P-*n*-O-PIMB derivatives **1a**–**1j**, **2a**–**2j**, **3a**–**3j** and **4a**–**4j**.

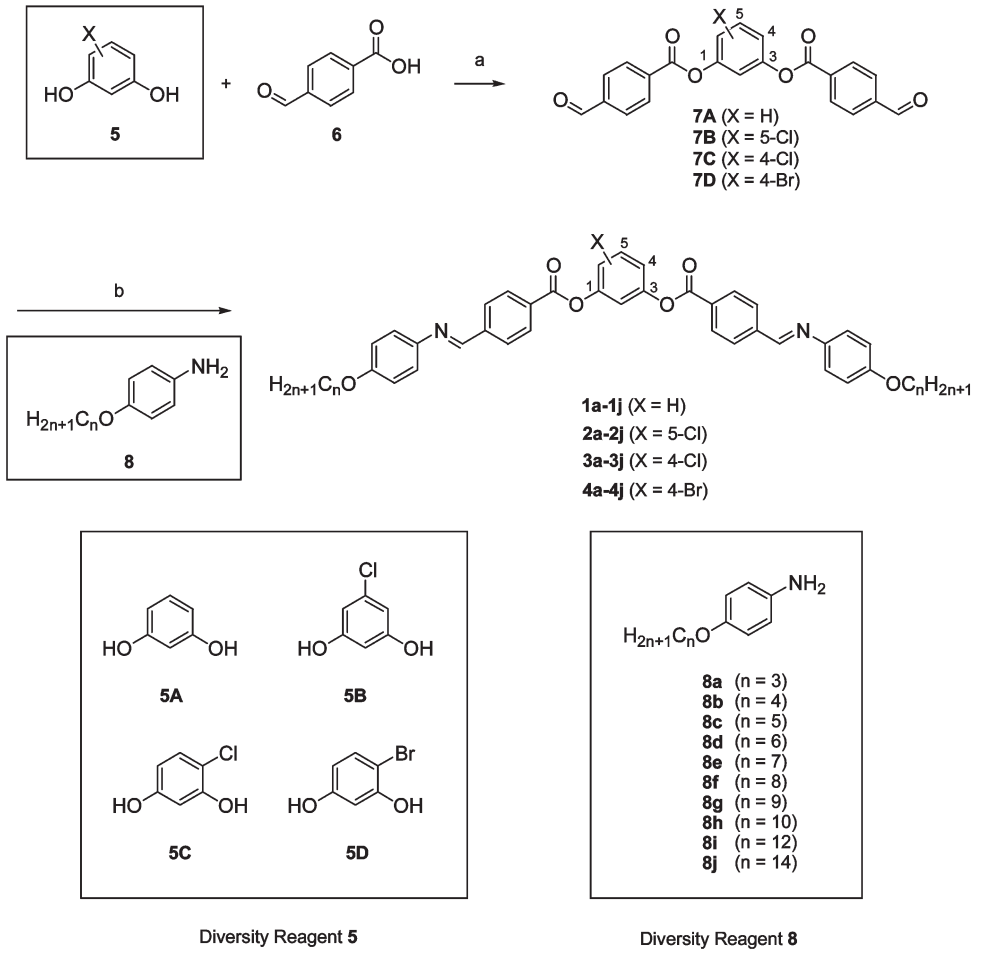

Scheme. Parallel synthesis of a 40-member combinatorial library of **1**–**4**. Reagents and conditions: (a) EDCI, CH_2Cl_2, rt, 24 h; (b) (i) ethanol, 60°C, 16 h, (ii) PS-TsNHNH$_2$[TM], $CHCl_3$.

2.2.2. *Synthesis of dialdehydes 7A–7D*

To four 50 ml reaction vessels placed on a Quest205[TM]† were added various resorcinol derivatives (1 mmol), 4-formylbenzoic acid (3 mmol) in dichloromethane (10 ml), 1-ethyl-3-(3-dimethylaminopropyl)carbodiimide hydrochloride (EDCI) (3 mmol), and diisopropylethylamine (DIEA) (3 mmol) under nitrogen. After agitation for 24 h at room temperature, each reaction mixture was quenched with water (10 ml) and the aqueous layer was extracted with ethyl acetate (15 ml). The organic extract was concentrated at 30°C by bubbling nitrogen to afford dialdehyde **7** as a dark solid, which was used for the next reaction without further purification. **7A** (X = H) ^{1}H NMR (270 MHz, $CDCl_3$) δ 7.21–7.26 (m, 3H), 7.53 (t, J = 8.1 Hz, 1H), 8.04 (d, J = 8.3 Hz, 4H), 8.27 (d, J = 8.6 Hz, 4H), 10.15 (s, 2H); **7B** (X = 5-Cl) ^{1}H NMR (270 MHz, $CDCl_3$) δ 7.19(t, J = 1.9 Hz, 1H), 7.27 (s, 2H), 8.00 (d, J = 8.3 Hz, 4H), 8.35 (d, J = 8.6 Hz, 4H), 10.16 (s, 2H); **7C** (X = 4-Cl) ^{1}H NMR (270 MHz, $CDCl_3$) δ 7.21(dd, J = 8.9 and 2.6 Hz, 1H), 7.34 (d, J = 2.6 Hz, 4H), 7.58 (d, J = 8.9 Hz, 4H), 8.02–8.06 (m, 4H), 8.35 (d, J = 8.3 Hz, 2H), 8.40 (d, J = 8.3 Hz, 2H), 10.15 (s, 1H), 10.16 (s, 1H); **7D** (X = 4-Br) ^{1}H NMR (270 MHz, $CDCl_3$) δ 7.16 (dd, J = 8.9 and 2.6 Hz, 1H), 7.13 (t, J = 2.6 Hz, 1H), 7.74 (d, J = 8.9 Hz, 1H), 8.02–8.07 (m, 4H), 8.35 (d, J = 8.3 Hz, 2H), 8.42 (d, J = 8.3 Hz, 2H), 10.15 (s, 1H), 10.16 (s, 1H).

†Quest 210 and 205 are parallel organic synthesizers (Argonaut Technologies). PS-TosNHNH2 was purchased from Argonaut Technologies, 1101 Chess Drive, Foster City, CA 94404

2.2.3. *Synthesis of P-n-O-PIMB derivatives **1a–1j**, **2a–2j**, **3a–3j** and **4a–4j***

Twelve 10 ml reaction vessels were placed on a Quest210[TM]. To the vessels were added the dialdehydes

7A–**7D** and 4-alkoxyphenylamine **8a**–**8j** (0.3 mmol) in ethanol (10 ml) under nitrogen, respectively. After agitation at 60°C for 16 h, each reaction mixture was filtered and the precipitate washed three times with hexane (10 ml × 3). The resulting solid was dissolved by chloroform and treated with the scavenger resins, PS-TsNHNH$_2$^{TM},to remove unreacted aldehydes **7**. Filtration and concentration provided crude products, which were successively purified by silica gel column chromatography in parallel using a COMBI FLASH^{TM}, gel permeation chromatography, and finally recrystallization from ethanol chloroform (10/1) to isolate **1**–**4** as colourless pure crystals (>95% purities) in 50–65% overall yields. NMR data for new compounds in this paper were in good agreement with the reported structures. Selected NMR data are given below.

4-Br-P-4-O-PIMB (**4b**). ^{1}H NMR (270 MHz, $CDCl_3$, δ) 0.99 (t, J=7.3 Hz, 6H), 1.44–1.57 (m, 4H), 1.74–1.85 (m, 4H), 4.00 (t, J=6.4 Hz, 4H), 6.95 (d, J=8.6 Hz, 4H), 7.15 (dd, J=8.6 and 2.6 Hz, 1H), 7.26–7.34 (m, 5H), 7.72 (d, J=8.9 Hz, 1H), 8.03 (d, J=8.3 Hz, 2H), 8.05 (d, J=8.3 Hz, 2H), 8.27 (d, J=8.3 Hz, 2H), 8.33 (d, J=8.3 Hz, 2H), 8.58 (s, 1H), 8.59 (s, 1H). ^{13}C NMR (67.8 MHz, $CDCl_3$, δ) 164.1, 163.5, 158.6, 156.1, 150.5, 148.7, 143.9, 143.8, 141.4, 141.3, 133.5, 130.8, 130.6, 130.3, 128.6, 122.5, 120.9, 117.9, 115.0, 113.0, 68.0, 31.3, 19.2, 13.9. IR (solid) 2954, 2872, 1737, 1587, 1507, 1468, 1246, 1067, 833 cm^{-1}.

4-Br-P-8-O-PIMB (**4f**). ^{1}H NMR (270 MHz, $CDCl_3$, δ) 0.89 (t, J=6.6 Hz, 6H), 1.28–1.50 (m, 20H), 1.77–1.83 (m, 4H), 3.99 (t, J=6.6 Hz, 4H), 6.95 (d, J=8.9 Hz, 4H), 7.15 (dd, J=8.6 and 2.6 Hz, 1H), 7.26–7.34 (m, 5H), 7.72 (d, J=8.6 Hz, 1H), 8.03 (d, J=8.3 Hz, 2H), 8.05 (d, J=8.6 Hz, 2H), 8.27 (d, J=8.3 Hz, 2H), 8.33 (d, J=8.6 Hz, 2H), 8.58 (s, 1H), 8.58 (s, 1H). ^{13}C NMR (67.8MHz, $CDCl_3$, δ) 164.1, 163.5, 158.5, 156.1, 150.5, 148.8, 143.9, 143.9, 141.4, 141.3, 133.5, 130.8, 130.6, 130.4, 128.6, 122.5, 120.8, 117.9, 115.1, 113.0, 68.4, 31.9, 29.6, 29.4, 29.3, 26.0, 22.7, 14.1. IR (solid) 2924, 2854, 1743, 1623, 1591, 1502, 1475, 1411, 1247, 1037, 835 cm^{-1}.

4-Br-P-14-O-PIMB (**4j**). ^{1}H NMR (270 MHz, $CDCl_3$, δ) 0.88 (t, J=6.6 Hz, 6H), 1.27–1.47 (m, 44H), 1.75–1.85 (m, 4H), 3.99 (t, J=6.6 Hz, 4H), 6.95 (d, J=8.9 Hz, 4H), 7.15 (dd, J=8.9 and 2.6 Hz, 1H), 7.26–7.34 (m, 5H), 7.72 (d, J=8.9 Hz, 1H), 8.03 (d, J=8.6 Hz, 2H), 8.05 (d, J=8.6 Hz, 2H), 8.27 (d, J=8.3 Hz, 2H), 8.33 (d, J=8.6 Hz, 2H), 8.58 (s, 1H), 8.58 (s, 1H). ^{13}C NMR (67.8 MHz, $CDCl_3$, δ) 164.0, 163.5, 158.5, 156.1, 150.5, 148.7, 143.8, 141.4, 133.5, 130.8, 130.6, 130.3, 128.6, 128.6, 122.5, 120.9, 117.9,

Table 1. Transition temperatures (°C) of the 4Br-P-*n*-O-PIMB series measured on cooling at a rate of 10°C min^{-1}. The transition enthalpies(-kJ mol^{-1}) are given in parentheses. The enthalpy of 4Br-P-9-O-PIMB refers to the sum of both I–B2 and B2–X1 phase transitions.

n	Cr		X_3		X_2		X_1		B*x*		B2		I
3[a]	•	114.3 (28.6)	—		—		—		•	130.9 (5.53)	—		•
4[b]	—		•	100.3 (17.9)	—		—		•	139.9 (7.12)	—		•
5	—		•	106.0 (17.6)	—		—		•	121.5 (6.95)	—		•
6	—		—		•	114.5 (25.9)	—		—		—		•
7	—		—		•	120.4 (27.5)	—		—		—		•
8	—		—		•	124.3 (22.7)	—		—		—		•
9	—		—		—		•	120.0 (29.1)	—		•	125.5	•
10	—		—		—		•	116.0 (19.1)	—		•	128.3 (13.8)	•
12	—		—		—		•	112.9 (24.4)	—		•	133.7 (17.1)	•
14	—		—		—		•	111.2 (28.7)	—		•	133.9 (15.9)	•

[a]Compound n=3 shows monotropic morphism, melting at 136.5°C on heating.

[b]Once compound n=4 is crystallized, it melts at 155.9°C (in the case of 1st heating also) which is remarkably higher than the clearing temperature of the B*x* phase (142.1°C) and X3–B*x* phase transition temperature (125.1°C) on heating. No crystallization takes place for the other compounds.

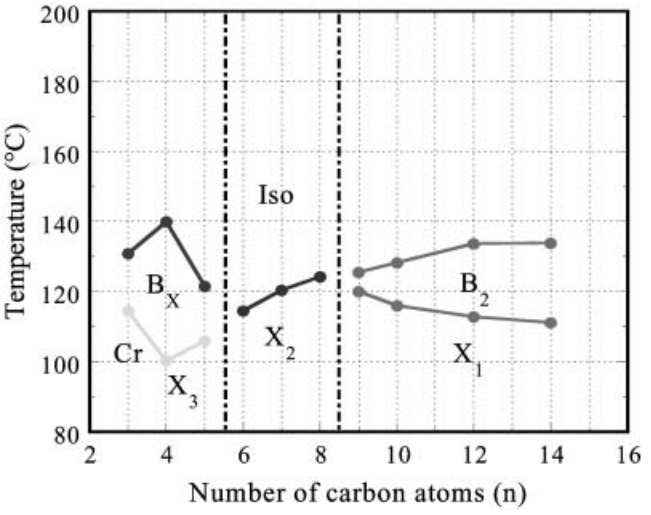

Figure 1. Phase diagram of 4Br-P-*n*-O-PIMB ($n = 3$–10,12,14) determined on cooling at a rate of $10^{\circ}C\,min^{-1}$. The materials are categorized into three groups, groups I, II and III, which show significantly different phase transition behaviours depending on the terminal chain length.

115.1, 113.0, 68.3, 31.9, 29.7, 29.6, 29.4, 29.3, 29.3, 26.0, 22.7, 14.1. IR (solid) 2921, 1732, 1623, 1505, 1473, 1412, 1272, 1153, 1074, 853 cm^{-1}.

3. Results and discussion

3.1. *Phase transition behaviour of 4Br-P-n-O-PIMB (**4**)*

As mentioned already, here, we compare the liquid crystallinity of the 4Br-P-*n*-O-PIMB series with the parent P-*n*-O-PIMB homologues. Every member of this series exhibits enantiotropic liquid crystalline phases, except for 4Br-P-3-O-PIMB. The phase transition temperatures and mesophase sequences of the 4Br-P-*n*-O-PIMB homologues determined on cooling are listed in table 1 and shown in figure 1. It can be seen in figure 1 that the materials exhibit three different types of mesophase dependeng on the number of carbons in the terminal chains. In order to simplify the discussion, we will group them into three categories: group I with longer terminal tails ($n = 9$, 10, 12, 14), group II with moderate terminal tails ($n = 6$, 7, 8) and group III with shorter terminal tails ($n = 3$, 4, 5). It is noted that the clearing temperatures increase when the number of carbons increases for group I, and are significantly lower than those for the parent analogues of the P-*n*-O-PIMB series [7].

For group I with longer terminal chains, the fluid smectic B2 phase appears on cooling from the isotropic melt and then undergoes a transformation to the highly ordered X1 phase. In group II, the fluid smectic B2 phase disappears, and they show only direct transition from the isotropic state to the X2 phase, which at first sight looks like the B4 phase found in the P-*n*-O-PIMB homologues. For group III with shorter terminal tails, the fluid smectic B*x* phase appears and then transforms to a crystalline phase. However, some of the compounds in group III exhibits the X3 phase, when the crystalline phase was annealed or with slow cooling from the B*x* phase. This complicated behaviour is clearly different from that observed in the P-*n*-O-PIMB series. A more detailed discussion of the mesomorphic behaviour of each group will now be given.

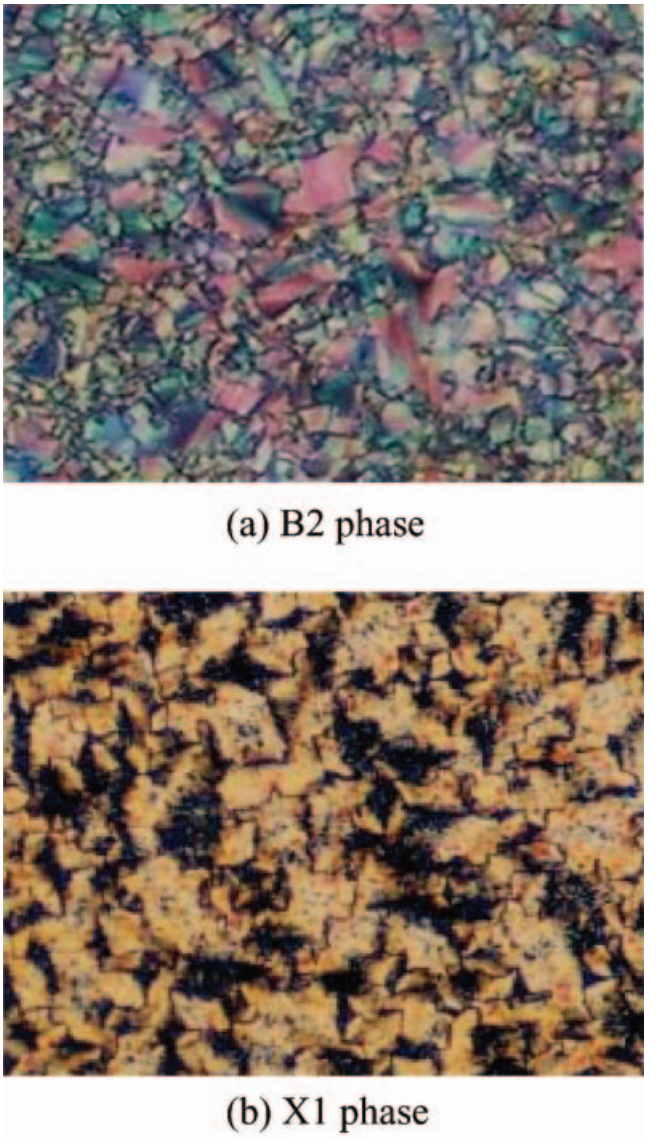

Figure 2. Polarizing optical microscopy textures of 4Br-P-14-O-PIMB; (*a*) the B2 phase and (*b*) the X1 phase.

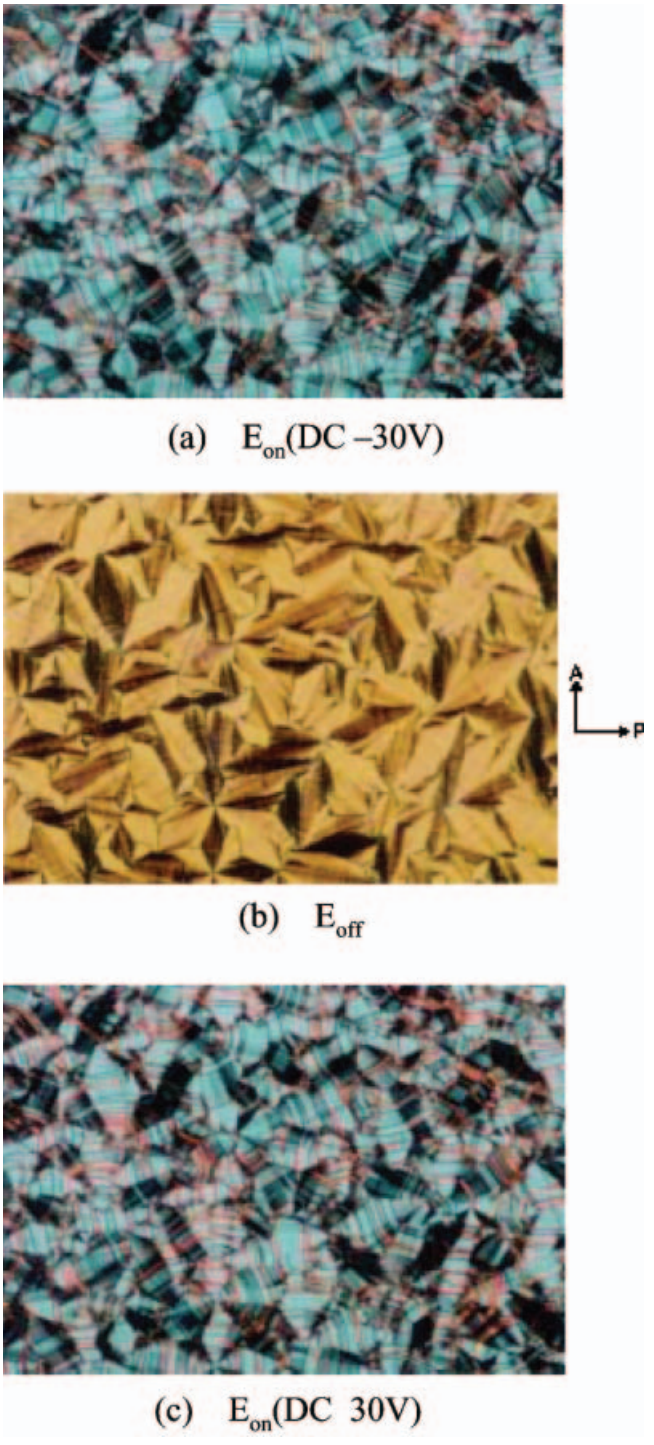

Figure 3. Polarizing optical microscopy textures for the B2 phase of 4Br-P-14-O-PIMB under application of an external electric field. In (*a*) and (*b*), observed with applied electric fields, the rotations of extinction brushes can be recognized from their positions without field (b), which correspond to the crossed polarization directions. This switching behaviour is the unique characteristic of antiferroelectric ordering with anticlinic layer structure of the B2 phase.

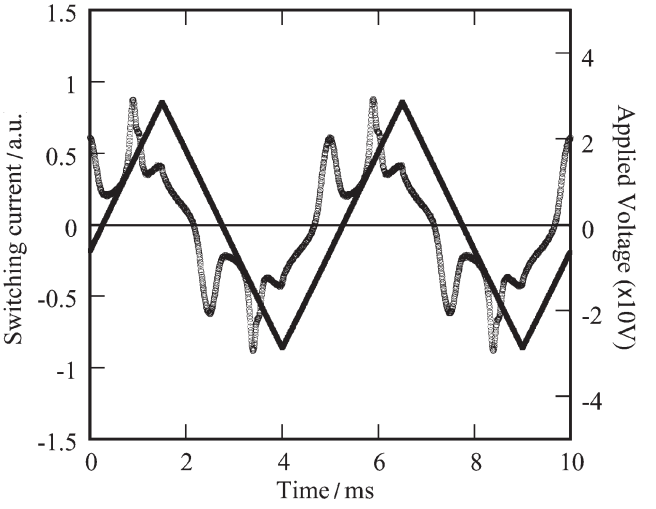

Figure 4. Reversal current responses to the applied triangular wave form on the B2 phase of 4Br-P-*n*-O-PIMB showing two peaks within the half cycle, which is characteristic of antiferroelectricity. A 6 μm cell was used under conditions of 65 V_{pp} and 100 Hz.

3.2. *Mesomorphic behaviour of 4Br-P-n-O-PIMB with longer terminal chains (group I: n = 9, 10, 12, 14)*

The phase sequence of this group is I–B2–X1. On cooling, many germ-like domains isolate from the isotropic matrix and finally coalesce to form a type of broken-fan texture as shown in figure 2 (*a*). This can be assigned as the B2 phase. The majority of the fan-textures are not striped, which is a characteristic of the homochiral layer structure of the B2 phase, either SmC_AP_A or SmC_SP_F structure, which is normally observed in the B2 phase of the P-*n*-O-PIMB homologues. In order to identify the type of layer structure, we carried out an electro-optic measurement by filling the samples into a 6 μm thick cell and applying an external electric field. The results are shown in figure 3. One can see that the extinction brushes rotate and the birefringent colour changes on applying the d.c. voltage. These are distinct characteristics of homochiral domains. In figure 4, the reversal current on applying a triangular waveform appears as two peaks, showing the antiferroelectricity of the B2 phase. Thus, we can conclude that the layer structure of the B2 phase in group I is SmC_AP_A. From WAXD data, the layer spacings of the B2 phase are 39.7, 42.6 and 45.2 Å for 4Br-P-10-O-PIMB, 4Br-P-12-O-PIMB and 4Br-P-14-O-PIMB, respectively. These spacings are relatively shorter than the most extended molecular length and very similar to those in the B2 phase of the parent P-*n*-O-PIMB molecules with the same terminal chain lengths. The tilt angle elucidated from the electro-optical microscopy is around 35°, which is also similar to that found in P-*n*-O-PIMB homologues. Thus, in this

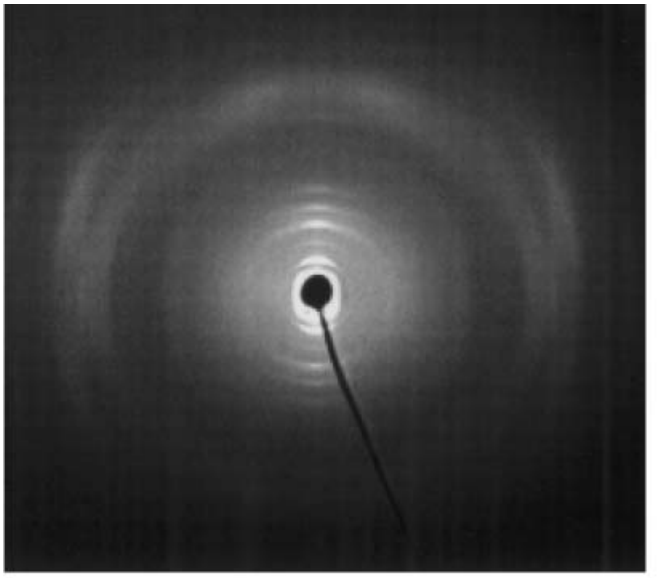

(a)

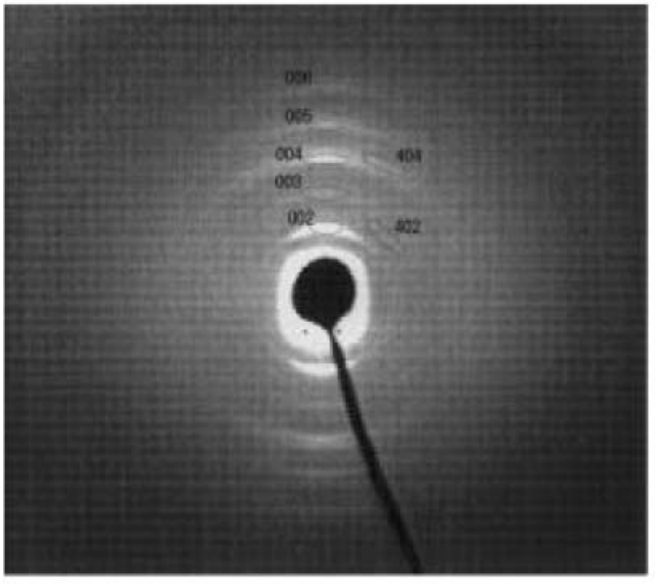

(b)

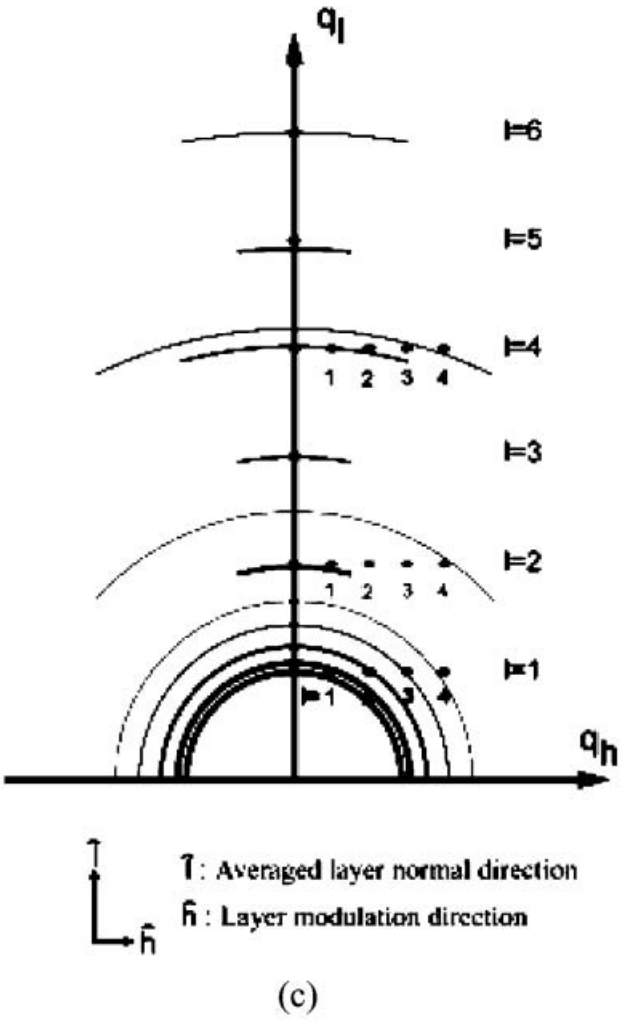

(c)

Figure 5. (*a*) Wide angle X-ray diffraction (WAXD) profile obtained from an aligned sample in the X1 phase for 4Br-P-*n*-O-PIMB. In addition to the (0 0 *l*) reflections, several other (*h* 0 *l*) reflections are observed, showing additional periodic order in the direction parallel to the layers. (*b*) Magnified WAXD pattern of the X1 phase with the layer reflections on the 0 0 *l* series and the weak intensity away from the meridian reflections marked. (*c*) Sketch of the diffraction pattern from a WAXD profile for the X1 phase.

B2 phase the molecular conformations and the tilting packing fashion are the same as those in the parent P-*n*-O-PIMB series.

The lower temperature X1 phase shows a weaker optical birefringence than the higher temperature B2 phase, as shown in figure 2 (*b*). It is apparently solid, but is different from a typical crystalline phase. Figure 5 (*a*) shows the WAXD pattern for an aligned sample of the X1 phase of 4Br-P-14-O-PIMB. Here, the alignment was initially prepared in the B2 phase by

Table 2. X-ray data for the X1 phase of 4Br-P-14-O-PIMB.

d_{obs}/Å	Intensity	Indices	d_{calc}/Å[a]
52.8	vs	0 0 1	52.9
48.8	vs	1 0 1	50.0
42.8	m	2 0 1	43.5
36.7	vw	3 0 1	36.7
31.8	vw	4 0 1	31.0
26.7	vs	0 0 2	26.5
21.2	vw	4 0 2	21.8
17.6	w	0 0 3	17.6
13.1	m	0 0 4	13.2
12.6	vw	4 0 4	12.5
10.7	w	0 0 5	10.6
8.80	vw	0 0 6	8.82

[a]Based on $a = 153$ Å and $c = 52.9$ Å, two-dimensional rectangular lattice.

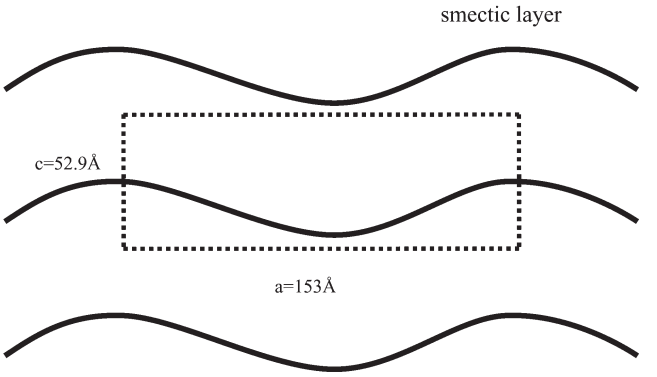

Figure 6. Layer undulation model of the X1 phase, which can be described as a long range two-dimensional rectangular ordering.

treating a glass surface with organosilane, as previously reported in [7]. One can see a number of regular layer line reflections on the 0 0 *l* series, indicating that the layer order essentially remains in the X1 phase. The layer thickness increases on the transformation from the B2 to X1 phase; 45.1, 49.1 and 52.9 Å for 4Br-P-10-O-PIMB, 4Br-P-12-O-PIMB and 4Br-P-14-O-PIMB, respectively. The broad diffuse diffraction pattern in the wide angle region indicates the liquid-like ordering of the phase. It is interesting to note that several additional weak intensities of the meridian, i.e. *h* 0 1, *h* 0 2 and *h* 0 4, appear in the WAXD pattern of the X1 phase, as can be seen in figures 5 (*a*) and 5 (*b*) for the magnified X-ray profile.

For clarity, a sketch of the diffraction pattern is shown in figure 5 (*c*). The layer spacings are listed in table 2. This X-ray pattern indicates that a density modulation takes place along the smectic layer, which has already been reported by Watanabe *et al.* for the structure of the B1 phase [4] and by Clark *et al.* for the B7 phase [28]. Their description involves a frustration of the ferroelectric structure. From the simple consideration of the layer reflections, there is a long range positional order of 153 Å in the direction of the smectic layer for 4Br-P-14-O-PIMB. The calculated spacings based on a unit lattice of $a = 153$ Å, $c = 52.9$ Å are compared with the observed ones in table 2, and good agreement can be seen between them.

One of the possible structures, the undulated structure, is sketched in figure 6. Recently, layer undulation in the B7 phase has been proposed as the molecular splay polarization model [28]. Irrespective of this ambiguity in the structure, it is obvious that a long range two dimensional order (i.e. layer undulation mode) in the X1 phase resulted from a subtle interaction to minimize the total macroscopic polarization.

3.3. *Mesomorphic behaviour of 4Br-P-n-O-PIMB with moderate terminal chains (group II: n = 6, 7, 8)*

In group II, the fluid B2 smectic phase disappears, and a highly viscous phase designated the X2 phase, which is assumed to possess a highly ordered structure, is directly formed from isotropic liquid: I–X2. The X2 phase shows an unidentified texture with extremely low birefringence, see figure 7 (*a*). Interestingly two different kinds of domain, with opposite optical rotations, can be clearly detected when the analyser or polarizer is rotated from the crossed position, as shown in figures 7 (*b*) and 7 (*c*). This is optically similar to the B4 phase in the parent P-*n*-O-PIMB homologues and leads to consideration of a helical and/or chiral superstructure for the X2 phase. However, it should be noted that there are also significant dissimilarities between the X2 and B4 phases with regard to their layer thicknesses and WAXD profiles. Specifically, the layer thicknesses for the B4 phase in the P-*n*-O-PIMB homologous series are approximately equal to the molecular lengths; i.e. 41.2, 43.5 and 45.7 Å for $n = 6$, 7 and 8, respectively [7]. In addition, the WAXD profile of the B4 phase indicates a strong correlation from layer to layer by the appearance of several strong intensity reflections on the 0 0 *l* series, figure 8 (*b*). By contrast, these are not seen for the X2 phase, figure 8 (*a*).

One can also differentiate the molecular interactions and/or the 3D ordering between the X2 and B4 phases using the wide angle diffraction patterns. The X2 phase in the 4Br-P-*n*-O-PIMB series is considered to have more liquid-like associations between the molecules than that for the B4 phase of the P-*n*-O-PIMB

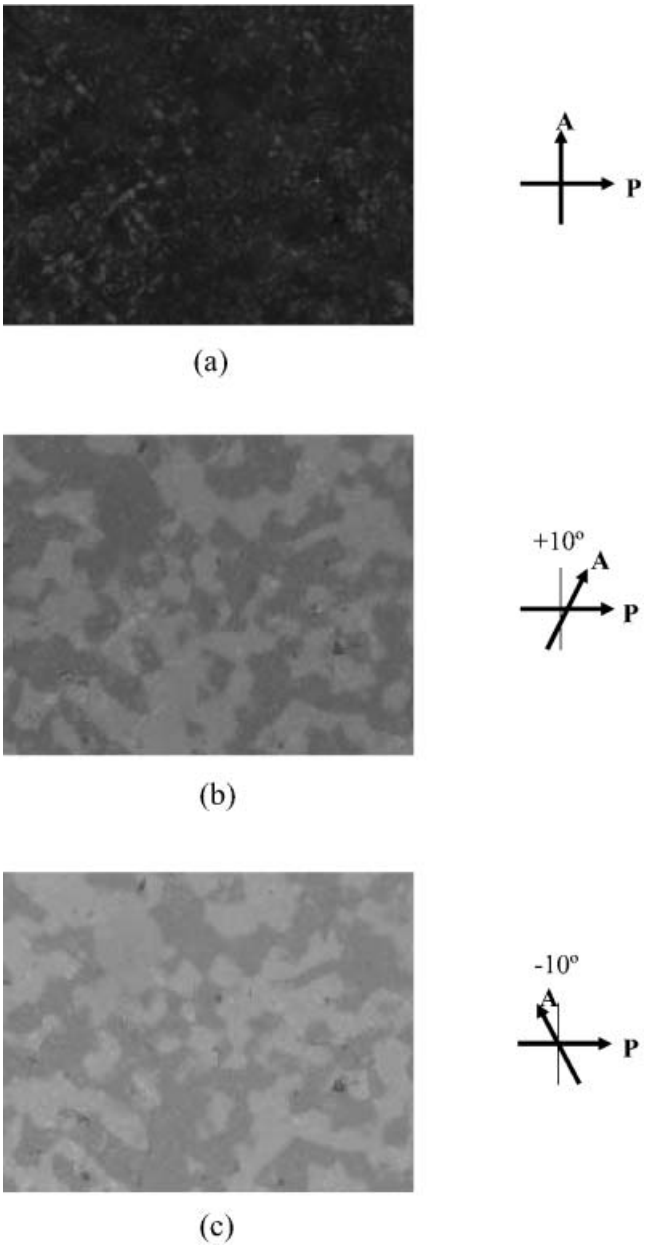

Figure 7. Polarizing optical microscopy texture observed in the X2 phase of 4Br-P-7-O-PIMB. In (*a*), the texture is observed under crossed polarizers, while textures in (*b*) and (*c*) are observed by 10° clockwise and counter-clockwise rotations of the analyser from the crossed position, respectively.

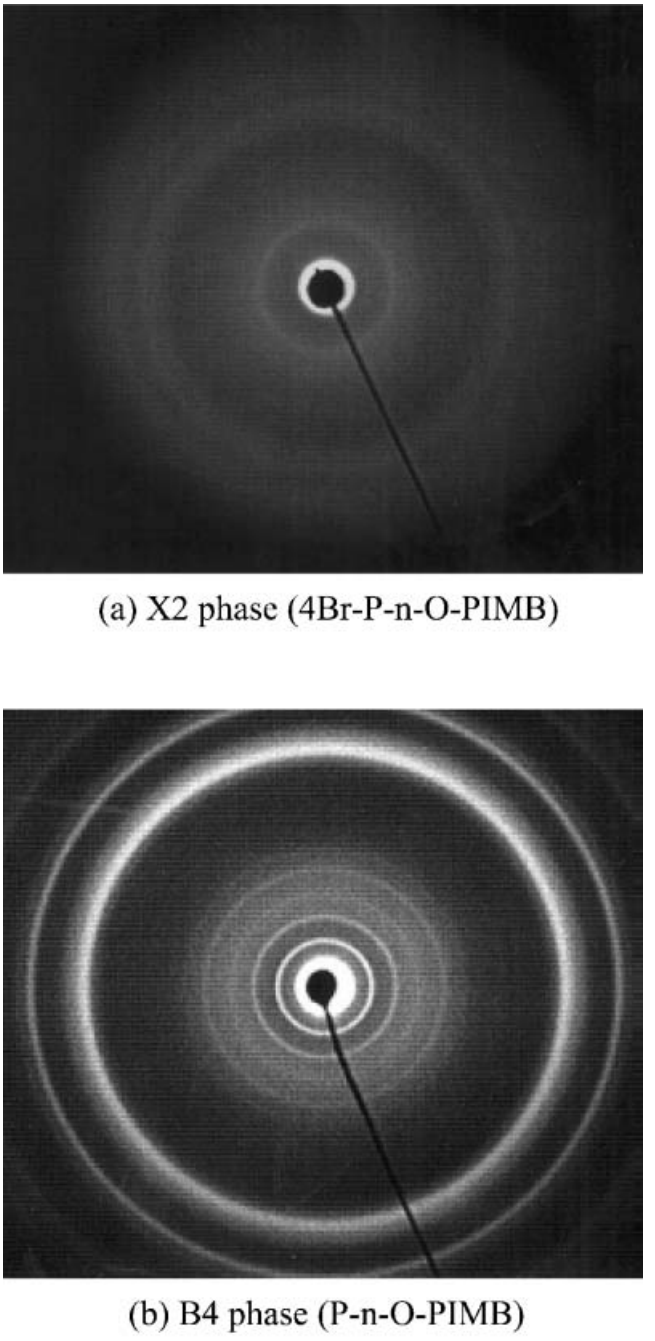

Figure 8. (*a*) WAXD profile of the X2 phase in the 4Br-P-*n*-O-PIMB series. (*b*) WAXD profile of the B4 phase in the parent P-*n*-O-PIMB homologous series.

homologues. Also, the layer thicknesses of the X2 phase, 34.8 Å in 4Br-P-6-O-PIMB, 35.9 Å in 4Br-P-7-O-PIMB and 37.0 Å in 4Br-P-8-O-PIMB, are relatively shorter than the molecular lengths. This implies that the molecules in the X2 phase are tilted within the layers and the tilt angle is roughly estimated to be about 34°.

3.4. *Mesomorphic behaviour of 4Br-P-n-O-PIMB with shorter terminal chains (group III: n = 3, 4, 5)*

This group shows two different mesophases, Bx and X3 phases and differs from the other groups, in that crystallization takes place if the X3 phase is annealed at below 80°C: I–Bx–X3–(Crystal). The fluid Bx phase exhibits clear focal-conic fan shaped textures as shown

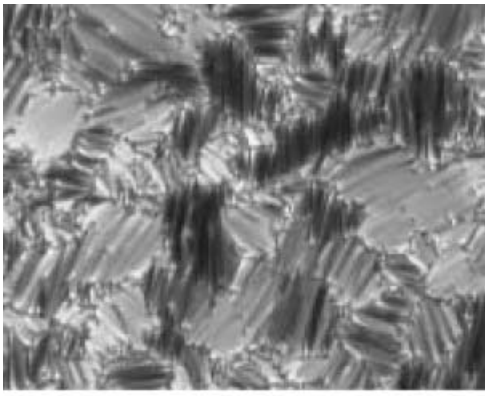

(a) Bx phase from isotropic

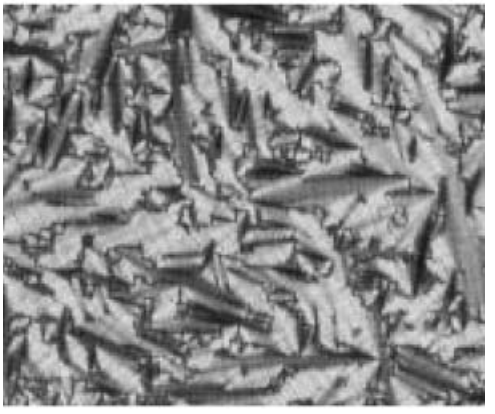

(b) X3 phase

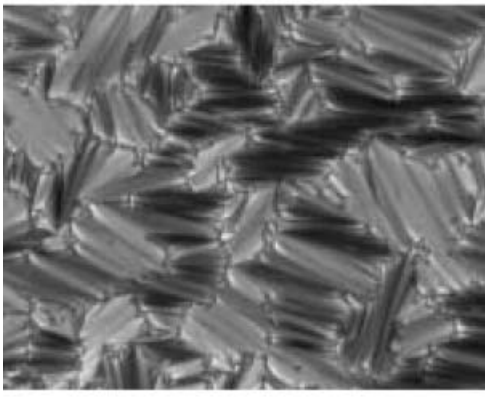

(c) Bx phase from X3 phase

Figure 9. Polarizing optical microscopy textures observed in the B*x* phase for 4Br-P-4-O-PIMB; (*a*) shows the typical fan-shaped texture of the Bx phase cooled directly from the isotropic melt, (*b*) shows the texture of the X3 phase at 90°C, as an appearance of clear stripes running across the fan-shaped domains. On heating to the Bx phase, the well defined fan-shaped texture reappears as in (*c*), but the optical axes of entire fan-shaped domains rotate by 90° with respect to the texture in (*a*).

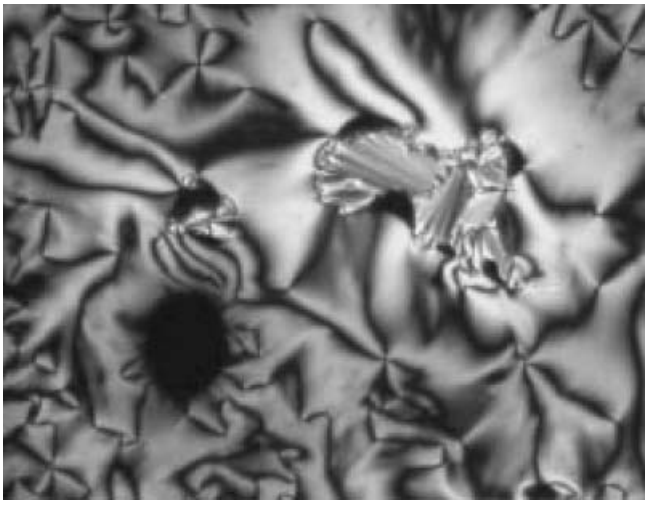

Figure 10. Polarizing optical microscopy texture observed for the homeotropically aligned B*x* phase of 4Br-P-4-O-PIMB. The schlieren texture is prepared in a surface-free condition, which is achieved by sliding a cover glass from an extremely thin sample. The existence of both two- and four-brush disclinations indicates the biaxiality of the B*x* phase.

in figure 9 (*a*). This texture can often be seen for SmA or SmC phases formed by calamitic molecules. In a homeotropically aligned domain, schlieren textures with two- and four-brush disclinations are observed, suggesting a biaxiality in the Bx phase, see figure 10. Regardless of the well defined focal-conic fan texture implying the smectic layer order, it is striking that no layer reflection is observed either by WAXD or SAXS spectroscopy, as shown in figures 11 (*a*) and 11 (*c*). Only diffuse scattering, which indicates liquid-like ordering of the phase, is detected, see figure 11 (*a*). Furthermore neither a ferro- nor antiferro-electric response is detected. On applying a d.c. voltage to the Bx phase, only a change in birefringence between ON and OFF states is recognized (see figure 12).

A number of smectic phases which exhibit the fan-shape texture, but no layer reflection, have been reported in some non-symmetric dimeric liquid crystals [29] and calamitic bolaamphiphiles [30]. The phenomenon has been explained by a disordered layer orientation or super-undulation of the smectic strata. Consequently, the disappearance of the layer reflection for the smectic Bx phase could be considered to be caused by the disordered undulation structure.

For 4Br-P-3-O-PIMB, crystallization takes place in the low temperature region just below the Bx phase. On the other hand, for 4Br-P-5-O-PIMB and 4Br-P-4-O-PIMB, when cooled to low temperatures the focal-conic fan domains of the Bx phase change into fan-like

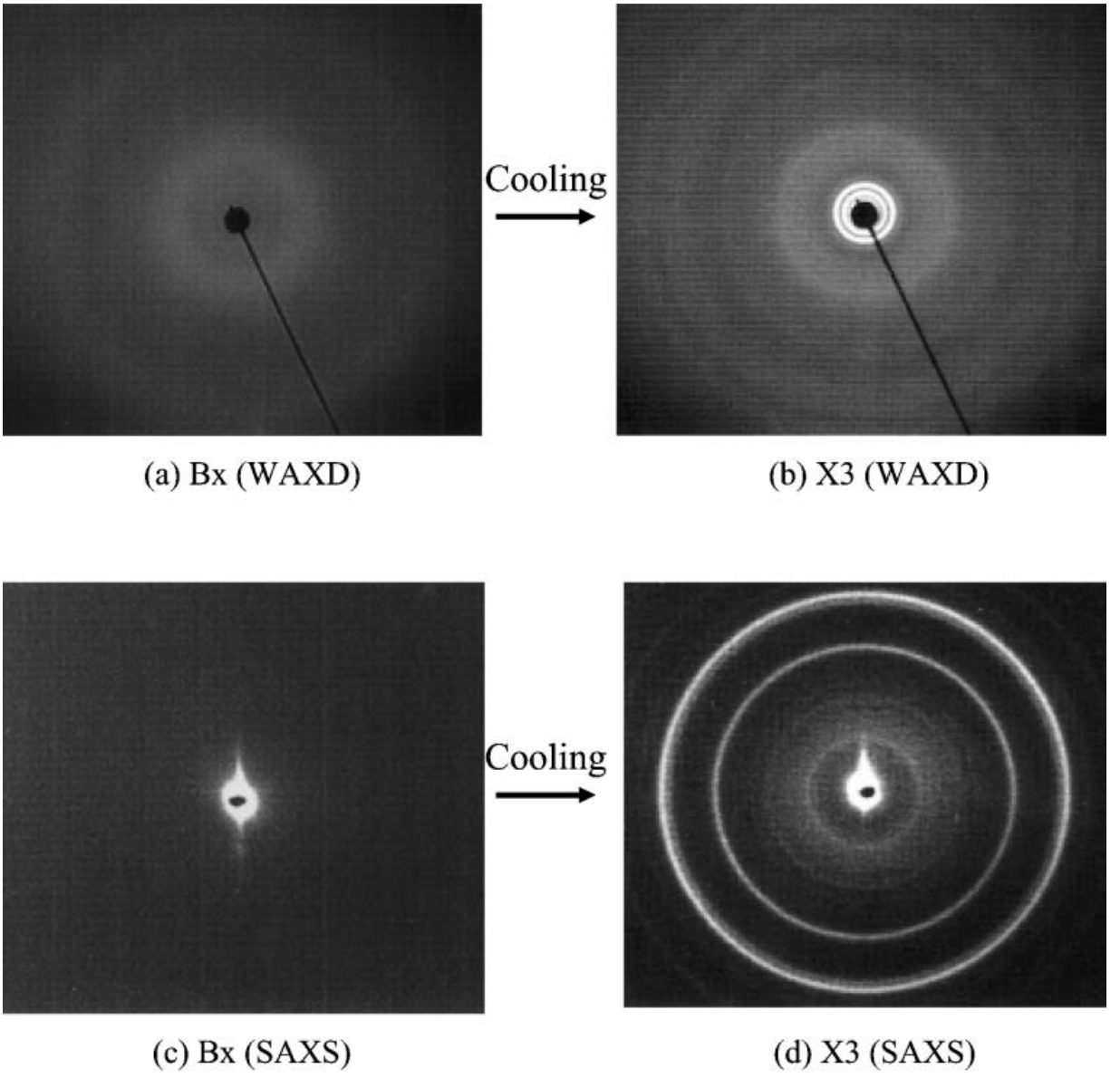

Figure 11. WAXD and SAXS profiles for the B*x* and X3 phase. (*a*) The WAXD profiles of the Bx phase obtained on cooling from isotropic state, (*b*) the WAXD profile of the X3 phase taken on further cooling from the Bx phase in the same sample, (*c*) the SAXS profile of the Bx phase on cooling from isotropic, (*d*) the SAXS profile for the X3 phase obtained on cooling from the Bx phase.

domains with sharp boundaries between each fan domain, and this is designated the X3 phase, see figure 9 (*b*). The domains include fine stripe patterns running across the fan backs. The X3 phase is a stable phase. It is interesting to note that it shows several reflections in both WAXD and SAXS regions, as shown in figures 11 (*b*) and 11 (*d*). As can be seen in the wide angle region of the WAXD profile, the X3 phase appears to have a liquid-like ordering, but the double diffuse scattering implies a more complicated molecular orientation than that found in the Bx phase. The calculated spacings from the SAXS profiles are listed in table 3.

We interpret the structure of the X3 phase by taking the diffraction analysis of the X-ray diffraction pattern as sketched in figure 13. We have found that the diffraction pattern detected can be well explained by a two-dimensional hexagonal lattice with the huge lattice parameter of ~ 120 Å. One possible model of the X3 phase is illustrated in figure 14. First, we suggest that the two-dimensional hexagonal order exists on the projection along the layers; no structure with a simple

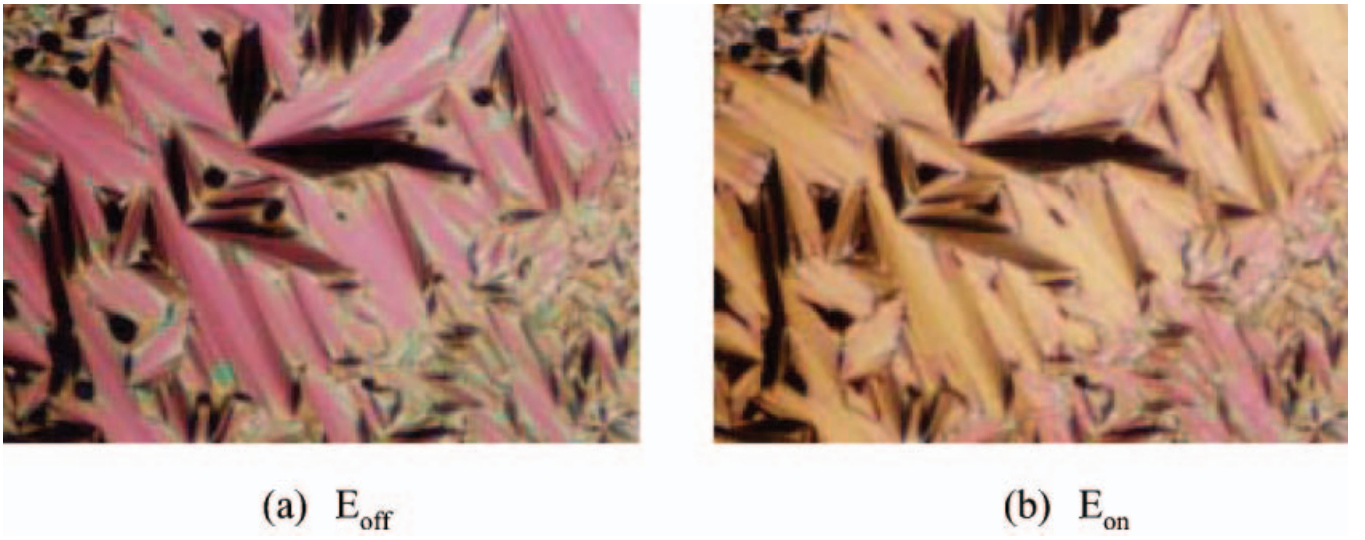

Figure 12. Polarizing optical microscopy textures observed in the Bx phase on applying a d.c. voltage of 60 V_{pp} to a 4 μm thick sample for 4Br-P-4-O-PIMB: (*a*) OFF state and (*b*) ON state. A switching current is undetectable, but a change of birefringence between ON and OFF states is recognized.

hexagonal symmetry can be envisaged on the projection perpendicular to the layer. In this model, the layers are divided into small pieces (or clusters) such that six clusters assemble with a circularly positional alignment in each unit lattice with an edge of 120 Å. Assuming that the density of the present system is 1 g cm^{-3} and that the lateral packing distance of molecules is 4.5 Å, we calculate that about 45 molecules are included in one unit lattice. Thus, each cluster is composed of seven or eight molecules on this projection. We suggest that this abnormal hexagonal structure is formed as the system minimizes its energy by escaping from macroscopic polarization.

Finally, we would like to show the interesting optical texture revolution for the Bx phase. As discussed earlier, the B*x* phase appears as fan-shaped domains on cooling from isotropic state, as can be seen in figure 9 (*a*). On the other hand, recovering the Bx phase by heating from the X3 phase also exhibits a well defined fan-shaped texture, as in figure 9 (*c*). However, the optical axes of the entire fan-shaped domains rotate by 90° with respect to the B*x* phase texture initially obtained from the isotropic state, as in figure 9 (*a*). The exact 90° rotation of the optical axis is reproducible under temperature cycling between the isotropic, Bx and X3 phases. This unusual change in the optical axis cannot be explained at present, but it essentially illustrates the exotic interrelationship between the Bx and X3 phases.

Table 3. X-ray data for the lower temperature X3 phase for 4Br-P-4-O-PIMB.

d_{obs}/Å	Intensity	Indices	d_{calc}/Å[a]
106.0	w	1 0 0	107.2
62.0	vw	1 1 0	62.0
53.7	vvw	2 0 0	53.7
		2 1 0	40.6
40.3	s	3 0 0	35.7
30.6	vw	2 2 0	31.0
29.8	s	3 1 0	29.8
		4 0 0	26.8
26.9	vw	3 2 0	24.6
23.7	w	4 1 0	23.4

[a]Based on two-dimensional hexagonal lattice with $a = b = 120$ Å.

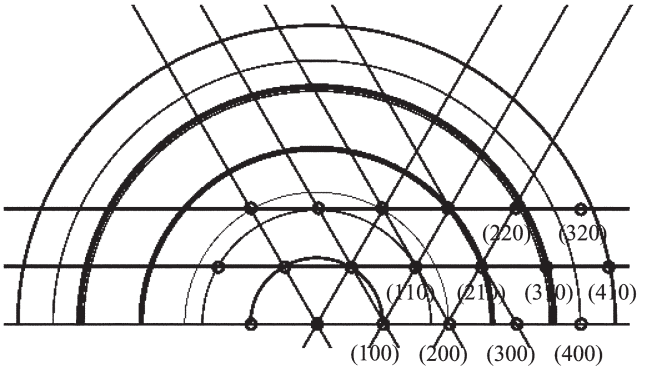

Figure 13. Sketch of the diffraction pattern for the X3 phase; the evaluation is made based on the X-ray data in figure 11.

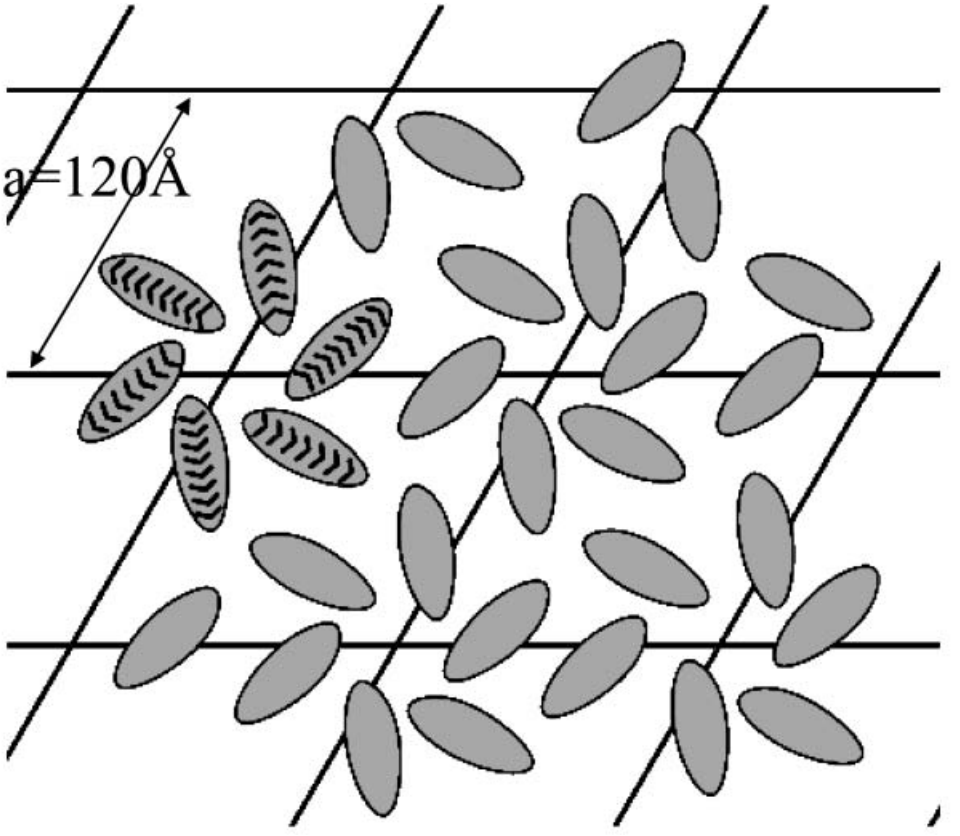

Figure 14. Illustration of a proposed structural model with a simple hexagonal symmetry in the X3 phase of 4Br-P-4-O-PIMB. The layers are broken into small pieces whereby about six clusters assemble on average into a unit lattice with a dimension of 120 Å. The grey domains indicate smectic clusters which are composed of a bunch of mesogens; the entire space around the smectic clusters is considered to be filled with flexible terminal chains.

4. Conclusion

A novel derivative series of the well known bent-shaped P-*n*-O-PIMB liquid crystal mesogens, referred to as 4Br-P-*n*-O-PIMB, 4Cl-P-*n*-O-PIMB, and 5Cl-P-*n*-O-PIMB, having a halogen atom on the phenyl ring at the central core, were readily synthesized by solution phase parallel synthesis based on a combinatorial approach. We have found interesting transitional behaviour for the 4Br-P-*n*-O-PIMB series, in which, the homologues with long side chains ($n=9$, 10, 12, 14) exhibited the homochiral and antiferroelectric B2 phase at higher temperatures and the X1 phase with a layer undulation structure on cooling. The molecules with alkyl chains of moderate length ($n=6$, 7, 8) form a chiral smectic X2 phase, which shows two clearly different domains having opposite optical rotations. For homologues with shorter terminal alkyl chain lengths ($n=3$, 4, 5), an unusual fluid smectic Bx phase is observed, which shows a focal-conic fan-shaped texture, but no layer reflections are observed. The lower temperature X3 phase in this group is also unusual as the molecules are packed into a huge hexagonal lattice with a lattice edge of 120 Å. We suggest that the lower temperature mesophases, X1, X2 and X3, are frustrated and/or helically ordered phases, which can be considered to be caused by a spontaneous escape from a macroscopic polarization. Thus, the types of the mesophases are strongly dependent on the terminal chain length, and their structures are more complicated when compared with the P-*n*-O-PIMB parent homologues. This suggests that the substitution of the bromine atom at the central core essentially creates a particular interaction between molecules, which in turn enhances a subtle intermolecular interaction in liquid crystalline phases. We are currently working on the chloro-substituted homologous series, and this will be comprehensively reported later.

References

[1] Niori, T., Sekine, T., Watanabe, J., Furukawa, T., and Takezoe, H., 1996, *J. mater. Chem.*, **6,** 1231.
[2] Niori, T., Sekine, T., Watanabe, J., Furukawa, T., and Takezoe, H., 1997, *Mol. Cryst. liq. Cryst.*, **301,** 337.
[3] Sekine, T., Takanishi, Y., Niori, T., Watanabe, J.,

and TAKEZOE, H., 1997, *Jpn. J. appl. Phys.*, **36,** L1201.
[4] WATANABE, J., NIORI, T., SEKINE, T., and TAKEZOE, H., 1998, *Jpn. J. appl. Phys.*, **37,** L139.
[5] Workshop on Banana-shaped Liquid Crystals: Chirality by achiral molecules; held in Berlin, December 1997.
[6] LINK, D. R., NATALE, G., SHAO, R., MACLENNAN, J. E., CLARK, N. A., KÖRBLOVA, E., and WALBA, D. M., 1997, *Science*, **278,** 1924.
[7] THISAYUKTA, J., TAKEZOE, H., and WATANABE, J., 2001, *Jpn. J. appl. Phys.*, **40,** 3277.
[8] PELZL, G., DIELE, S., and WEISSFLOG, W., 1999, *Adv. Mater.*, **11,** 707.
[9] WEISSFLOG, W., NÁDASI, H., DUNEMANN, U., PELZL, G., DIELE, S., EREMIN, A., and KRESSE, H., 2001, *J. mater. Chem.*, **11,** 2748.
[10] PELZL, G., DIELE, S., GRANDE, S., JÁKLI, A., LISCHKA, CH., KRESSE, H., SCHMALFUSS, H., WIRTH, I., and WEISSFLOG, W., 1999, *Liq. Cryst.*, **26,** 401.
[11] DEHNE, H., POETTER, M., SOKOLOWSKI, S., WEISSFLOG, W., DIELE, S., PELZL, G., WIRTH, I., KRESSE, H., and GRANDE, S., 2001, *Liq. Cryst.*, **28,** 1269.
[12] WEISSFLOG, W., KOVALENKO, L., WIRTH, I., DIELE, S., PELZL, G., SCHMALFUSS, H., and KRESSE, H., 2000, *Liq. Cryst.*, **27,** 677.
[13] KOVALENKO, L., WEISSFLOG, W., GRANDE, S., DIELE, S., PELZL, G., and WIRTH, I., 2000, *Liq. Cryst.*, **27,** 683.
[14] WIRTH, I., DIELE, S., EREMIN, A., PELZL, G., GRANDE, S., KOVALENKO, L., PANCENKO, N., and WEISSFLOG, W., 2001, *J. mater. Chem.*, **11,** 1642.
[15] WEISSFLOG, W., LISCHKA, CH., DIELE, S., PELZL, G., and WIRTH, I., 1999, *Mol. Cryst. liq. Cryst.*, **328,** 101.
[16] PELZL, G., DIELE, S., JÁKLI, A., LISCHKA, CH., WIRTH, I., and WEISSFLOG, W., 1999, *Liq. Cryst.*, **26,** 135.
[17] SEKINE, T., NIORI, T., SONE, M., WATANABE, J., CHOI, S. W., TAKANISHI, Y., and TAKEZOE, H., 1997, *Jpn. J. appl. Phys.*, **36,** 6455.
[18] THISAYUKTA, J., NAKAYAMA, Y., KAWAUCHI, S., TAKEZOE, H., and WATANABE, J., 2000, *J. Am. chem. Soc.*, **122,** 7441.
[19] HEPPKE, G., and MORO, D., 1998, *Science*, **279,** 1872.
[20] KUROSU, H., KAWASAKI, M., HIROSE, M., YAMADA, M., KANG, S., THISAYUKTA, J., SONE, M., TAKEZOE, H., and WATANABE, J., 2004, *J. phys. Chem. A*, **108,** 4674.
[21] ZENNYOJI, M., TAKANISHI, Y., ISHIKAWA, K., THISAYUKTA, J., WATANABE, J., and TAKEZOE, H., 2001, *Mol. Cryst. liq. Cryst.*, **366,** 693.
[22] SHILOV, S. V., RAUCH, S., SKUPIN, H., HEPPKE, G., and KREMER, F., 1999, *Liq. Cryst.*, **26,** 1409.
[23] IMASE, T., KAWAUCHI, S., and WATANABE, J., 2001, *J. mol. Struct.*, **560,** 275.
[24] NIWANO, H., NAKATA, M., THISAYUKTA, J., LINK, D. R., TAKEZOE, H., and WATANABE, J., *J. phys. Chem.* (in press).
[25] WILSON, S. R., and CZARNIK, A. W. (editors), 1997, *Combinatorial Chemistry –Synthesis and Application* (New York: John Wiley).
[26] HSIEH-WILSON, L. C., XIANG, X. D., and SCHULTZ, P. G. 1996, *Acc. chem. Res.*, **29,** 164.
[27] JANDELEIT, B., SCHAEFER, D. J., POWERS, T. S., TURNER, H. W., and WEINBER, W. H., 1999, *Angew. Chem. int. Ed.*, **38,** 2494.
[28] COLEMAN, D. A., FERNSLER, J., CHATTHAM, N., NAKATA, M., TAKANISHI, Y., KÖRBLOVA, E., LINK, D. R., SHAO, R., JANG, W. G., MACLENNAN, J. E., MONDAINN-MONVAL, O., BOYER, C., WEISSFLOG, W., PELZL, G., CHEN, L.-C., ZASADZINSKI, J., WATANABE, J., WALBA, D. M., TAKEZOE, H., and CLARK, N. A., 2003, *Science*, **301,** 1204.
[29] YOSHIZAWA, A., YAMAMOTO, K., DEWA, H., NISHIYAMA, I., YAMAMOTO, J., and YOKOYAMA, H., 2003, *J. mater. Chem.*, **13,** 172.
[30] KÖLBEL, M., BEYERSDORFF, T., CHENG, X. H., TSCHIERSKE, C., KLAIN, J., and DIELE, S., 2001, *J. Am. chem. Soc.*, **123,** 6809.